Proceedings of Fifth International Conference on **Enhanced, Compact and Ultra-Compact Heat Exchangers: Science, Engineering and Technology**, Eds. R.K. Shah, M. Ishizuka, T.M. Rudy, and V.V. Wadekar, Engineering Conferences International, Hoboken, NJ, USA, September 2005.

CHE2005 – 05

Numerical Simulation and Experimental Study of Flow and Heat Transfer Characteristics of Shell Side Fluid in Shell-and-Tube Heat Exchangers

Y.L.He [1], W.Q.Tao [2], B.Deng [3], X.Li [4] and Y.Wu [5]

1.Xi'an Jiaotong University, Xi'an, Shaanxi, China; yalinghe@mail.xjtu.edu.cn
2.Xi'an Jiaotong University, Xi'an, Shaanxi, China; wqtao@mail.xjtu.edu.cn
3.Xi'an Jiaotong University, Xi'an, Shaanxi, China; dengbin@mail.xjtu.edu.cn
4.Xi'an Jiaotong University, Xi'an, Shaanxi, China; Lizhiting_614@sohu.com
5.Xi'an Jiaotong University, Xi'an, Shaanxi, China; wuyangcom@sina.com

ABSTRACT

A three-dimensional, staggered grid, full–implicit control-volume based numerical model was presented for the analysis of laminar and turbulent fluid flow and heat transfer of shell side fluid in shell-and-tube heat exchangers. The numerical model used the distributed resistance method along with the concept of volumetric porosities, surface permeabilities to account for the presence of tubes in the heat exchangers. A modified $k-\varepsilon$ model was used to account for the effects of tubes on turbulence generation and dissipation. The wall function approach was used to deal with the near wall region. The three-dimensional model was validated by comparison of the computed pressure drop and heat transfer with some experiment data available obtained in the authors' group. Good agreement between the simulation results and experimental data is obtained. It shows that applying the three-dimensional numerical model with the modified $k-\varepsilon$ model can effectively simulate the turbulence fluid flow and heat transfer in shell-and-tube heat exchangers. The anisotropic porosities model can simulate the flow characteristics in the shell-side of heat exchangers more effectively than the existing isotropic porous medium model.

INTRODUCTION

Shell-and-tube heat exchanger are widely used in process industries. Good understanding of the flow, and temperature fields within a heat exchangers is required for the design of reliable and efficient units. This information can be gained either by experimental testing (Bell, 1963; Halle et al. 1984; Pletcher and Andrews,1994) or by simple analysis method (Tinker,1958; Palen and Taborek,1969). The methods of calculating the fluid resistance and heat transfer in the shell-and-tube heat exchangers , put forward by Tinker (1958) and Palen and Taborek(1969) are fully based on the correlations which drafted by the experiment data. However, the above methods can't predict the detailed flow, temperature, and turbulence fields in heat exchangers, rather, they can only give overall pressure drop and heat transfer rate. The detailed field values of velocity, temperature, and turbulence intensity are crucial for a better understanding of heat exchanger operation, and for studies in the design of heat exchangers. Usually, experimental testing is very expensive and time consuming. In addition, flow visualization and detailed turbulence measurements in heat exchangers are difficult to perform. Therefore, numerical simulation provides a useful alternative and a properly validated numerical model for shell-and-tube heat exchangers can serve as a cost effective research tool.

The numerical research for heat exchangers of single-phase and two-phase fluids has been developing continuously, since the piniering work of Patankar and Spalding in 1974,and later enhanced by Butterworth(1978), Patankar (1984), Sha (1982,1985), Prithiviraj and Andrews (1998a,1998b),and so on. The numerical simulation of single-phase flow in the heat exchangers is the base for studying the even more complicated heat exchangers, such as the condenser, evaporator, etc.

The actual shell side fluid flow is so complicated that even for the present-day computational resource it is still prohibitive for most researchers to resolute the flow details by field numerical simulation. On the other hand, by using simplified model proposed by Patankar and Spalding (1974) we can still obtain some useful information while keep the requirement of computer resources in the limitation that is acceptable by engineering computation. The basic idea of Patankar and Spalding approach is viewing the shell side structure as a nominal porous medium and the presence of the tubes and baffles are taken into account by introducing parameters as volume porosity and surface permeability. In addition, the friction effect caused by the existence of the

solid region is taken into account by introducing empirical friction factor data as an additional source term in the momentum equation. This approach, even though relied on empirical friction data, provides an practical method to numerically simulate the shell-side performance and has been widely adopted since its publication.

In this paper, a three-dimensional, fully implicit, numerical method is used to simulate the shell-side single phase fluid flow and heat transfer. The simulation model is based on the distributed resistance concept along with a porous medium model. This model has been used to predict the shell-side performance of three kinds of shell-and-tube heat exchangers: bare tube banks with mormal baffle, bare tube banks with helical baffle, and finned tube banks. All these research results have been compared with the experiment data available to the authors and reasonably good agreement between the simulation results and experimental data was obtained.

PHYSICAL MODEL

Porous Medium Model

Figure 1 shows a control volume that contains tubes. In the figure S is the total border surface area and $S = S_{ss} + S_{ff}$,where S_f is the total fluid surface area. $S_f = S_{fs} + S_{ff}$. S_{ff}, S_{fs}, S_{ss} are the border between the fluid and fluid, the border between the fluid and solid, and that between solid and solid, respectively. Let V be the volume of the control volume, which includes fluid and solid parts, V_f the volume occupied by fluid in the control volume, and V_s the volume occupied by solid in the same control volume.

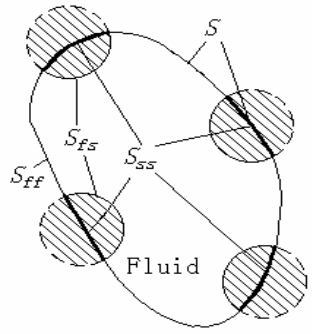

Fig. 1 Sample control volume with tubes

The volume porosity is a scalar quantity and can be determined as follows:

$$f_V = \frac{V_f}{V_f + V_S} = \frac{V_f}{V} \tag{1}$$

The surface permeabilities is a vector to account for the fluid surface area blocked by the solid structure (Sha, 1982), whose three components in $\vec{i}, \vec{j}, \vec{k}$ directions can be defined as follows:

$$f_x = \frac{\vec{S}_{ff} \cdot \vec{i}}{(\vec{S}_{ff} + \vec{S}_{ss}) \cdot \vec{i}}; f_z = \frac{\vec{S}_{ff} \cdot \vec{k}}{(\vec{S}_{ff} + \vec{S}_{ss}) \cdot \vec{k}} f_y = \frac{\vec{S}_{ff} \cdot \vec{j}}{(\vec{S}_{ff} + \vec{S}_{ss}) \cdot \vec{j}} \tag{2}$$

Governing Equations

For an arbitrary volume *V,* with boundary surface *S,* fluid density ρ , surface flux *J* and body source S_ϕ of any quantity ϕ , the general balance equation may be written as:

$$\frac{d}{dt}\int_V \rho\phi dV = -\int_S \vec{n} \cdot \vec{J} dS + \int_V S_\phi dV \tag{3}$$

By applying the Reynolds transport theorem and Gauss' theorem to the Eq.(3), the following general differential balance equation can be obtained:

$$\frac{\partial(\rho\phi)}{\partial t} + \nabla \cdot \rho\vec{u}\phi = -\nabla \cdot \vec{J} + S_\phi \tag{4}$$

Integrating Eq. (4) over the fluid part of the control volume as shown in Fig. 1, and introducing the definition of volume porosity, surface permeabilities and distributed resistance, Eq. (4) can be simplified and expressed in the differential form as:

$$\frac{\partial}{\partial t}(\rho f \phi) + \nabla \cdot (f \rho\phi\vec{V} - f\Gamma_\phi \nabla\phi) = fS_\phi \tag{5}$$

where f in the first term of the left hand side and the right hand side is the volume porosity, while that in the divergence term is the surface permeability.

In the cylindrical coordinates, the corresponding governing equations for mass, momentum and energy can be expressed by Eq.(6), where the source terms in the momentum and energy equations are listed in Table 1. In the table, k and ε are the kinetic energy and dissipation rate of turbulent kinetic energy in the $k-\varepsilon$ turbulence model. For the simplicity of presentation, the governing equations for k and ε are not shown in Eq.(6). The term T_s, T_t are the fluid temperatures of shell-side and tube side, and their source terms will be explained in the later discussion.

In the following the boundary conditions are illustrated for different kinds of the boundaries.

$$
\left.
\begin{aligned}
&\frac{\partial}{\partial t}(f_V\rho)+\frac{1}{r}\frac{\partial}{\partial\theta}(f_\theta\rho u)+\frac{1}{r}\frac{\partial}{\partial r}(f_r\rho rv)+\frac{\partial}{\partial z}(f_z\rho w)=0\\
&\frac{\partial}{\partial t}(f_V\rho u)+\frac{1}{r}\frac{\partial}{\partial\theta}(f_\theta\rho uu)+\frac{1}{r}\frac{\partial}{\partial r}(f_r r\rho vu)+\frac{\partial}{\partial z}(f_z\rho wu)=\\
&\quad\frac{1}{r}\frac{\partial}{\partial\theta}(\frac{\eta f_\theta}{r}\frac{\partial u}{\partial\theta})+\frac{1}{r}\frac{\partial}{\partial r}(\eta f_r r\frac{\partial u}{\partial r})+\frac{\partial}{\partial z}(\eta f_z\frac{\partial u}{\partial z})+S_u f_V\\
&\frac{\partial}{\partial t}(f_V\rho v)+\frac{1}{r}\frac{\partial}{\partial\theta}(f_\theta\rho uv)+\frac{1}{r}\frac{\partial}{\partial r}(f_r r\rho vv)+\frac{\partial}{\partial z}(f_z\rho wv)=\\
&\quad\frac{1}{r}\frac{\partial}{\partial\theta}(\frac{\eta f_\theta}{r}\frac{\partial v}{\partial\theta})+\frac{1}{r}\frac{\partial}{\partial r}(\eta f_r r\frac{\partial v}{\partial r})+\frac{\partial}{\partial z}(\eta f_z\frac{\partial v}{\partial z})+S_v f_V\\
&\frac{\partial}{\partial t}(f_V\rho w)+\frac{1}{r}\frac{\partial}{\partial\theta}(f_\theta\rho uw)+\frac{1}{r}\frac{\partial}{\partial r}(f_r r\rho vw)+\frac{\partial}{\partial z}(f_z\rho ww)=\\
&\quad\frac{1}{r}\frac{\partial}{\partial\theta}(\frac{\eta f_\theta}{r}\frac{\partial w}{\partial\theta})+\frac{1}{r}\frac{\partial}{\partial r}(\eta f_r r\frac{\partial w}{\partial r})+\frac{\partial}{\partial z}(\eta f_z\frac{\partial w}{\partial z})+S_w f_V\\
&\frac{\partial}{\partial t}(f_V\rho T)+\frac{1}{r}\frac{\partial}{\partial\theta}(f_\theta\rho uT)+\frac{1}{r}\frac{\partial}{\partial r}(f_r r\rho vT)+\frac{\partial}{\partial z}(f_z\rho wT)=\\
&\quad\frac{1}{r}\frac{\partial}{\partial\theta}(\frac{\lambda f_\theta}{c_p r}\frac{\partial T}{\partial\theta})+\frac{1}{r}\frac{\partial}{\partial r}(\frac{\lambda}{c_p}f_r r\frac{\partial T}{\partial r})+\frac{\partial}{\partial z}(\frac{\lambda}{c_p}f_z\frac{\partial T}{\partial z})+S_T f_V
\end{aligned}
\right\}\quad(6)
$$

Table 1 Source terms in the governing equations

ϕ	Γ_ϕ	S_ϕ
u	η	$-\frac{\rho V_r V_\theta}{r}+2\frac{\eta}{r^2}\frac{\partial V_r}{\partial\theta}-\frac{\eta V_\theta}{r^2}-\frac{\partial\overline{p}}{\partial\theta}+\rho g_\theta+R_\theta$
v	η	$\frac{\rho V_\theta^2}{r}-2\frac{\eta}{r^2}\frac{\partial V_\theta}{\partial\theta}-\frac{\eta V_r}{r^2}-\frac{\partial\overline{p}}{\partial\theta}+\rho g_r+R_r$
w	η	$-\frac{\partial\overline{p}}{\partial z}+\rho g_z+R_z$
T_s	$\frac{\mu}{\mathrm{Pr}}+\frac{\mu_t}{\mathrm{Pr}_t}$	$\frac{U_0 A_s}{V}\left(\frac{H_{\mathrm{tube}}}{C_{\mathrm{Ptube}}}-\frac{H_{\mathrm{shell}}}{C_{\mathrm{pshell}}}\right)$
T_t	-	$-\frac{U_0 A_s}{V}\left(\frac{H_{\mathrm{tube}}}{C_{\mathrm{Ptube}}}-\frac{H_{\mathrm{shell}}}{C_{\mathrm{pshell}}}\right)$
k	$\frac{\mu_r}{\sigma_k}$	$G-\rho\varepsilon+R_k$
ε	$\frac{\mu_r}{\sigma_\varepsilon}$	$C_1 G\frac{\varepsilon}{k}-C_2\rho\frac{\varepsilon^2}{k}+R_\varepsilon$

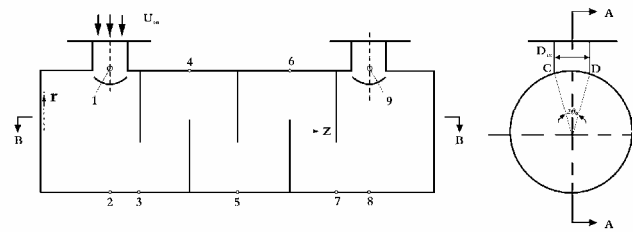

Fig. 2 Shell-and-tube HEx with normal baffles

Inlet Boundary Condition

Take a shell and tube heat exchanger with normal baffles as an example (Fig. 2). The on coming velocity U_{in} is known to be vertically downward, and the inlet domain is the section where the shell surface and the inlet tube surface intersect, which is characterized by $\theta<\theta_0$, and $r<r_{in}$. For this region the three velocity components can be determined as follows:

$$
\begin{cases}
u=u_{in}\cdot sin\theta\\
v=-u_{in}\cdot cos\theta\\
w=0
\end{cases}
\qquad(7)
$$

The inlet temperatures of shell side fluid and tube side fluid are pre-specified. The inlet kinetic energy for turbulent flow is taken as 1% of the kinetic energy of the on coming flow and the dissipation ε is determined by following two equations:

$$
\begin{aligned}
&2\rho u_m R_{in}/\eta_t=500\\
&\eta_t=C_u\rho k^2/\varepsilon
\end{aligned}
\qquad(8)
$$

Outlet Boundary Condition The definition of the outlet region is the same as the inlet region except for the axial location. For the velocity component which is normal upward, the mass conservation condition is used to determine the outlet value from the adjacent inner point. The details for this treatment can be found in Tao(2001). At the outlet the other two components are treated as fully developed, i.e., their first derivatives with respect to radius equals zero. The same treatment is adopted for the shell side fluid temperature, kinetic energy and the dissipation term.

Symmetry Surface On the symmetric surface where $\theta=0$ and $\theta=\pi$ following condition applies:

$$
u=0\ ,\ \frac{\partial V}{\partial\theta}\ ,\ \frac{\partial w}{\partial\theta}=0
\qquad(9)
$$

Solid Wall On all solid walls for velocity no slip boundary condition is applied, and for temperature the adiabatic condition is adopted.

Distributed Resistances

Based on the flow in anisotropic porosity media, under the cylindrical coordinates, distributed resistance can be defined as three parts: radius flow R_r, circumferential flow R_θ and axial flow R_Z. For the bare tube banks, Zukahauskas conducted experiments on tubes in cross flow and obtained pressure correlations. Base on these test data, the distributed resistances R_r and R_θ are formulated as:

$$
R_r=(\frac{\Delta p}{\Delta r})_r=0.5\frac{1}{\Delta r}N_L\rho\kappa F V_{r\max}^2
\qquad(10)
$$

$$R_\theta = (\frac{\Delta p}{r\Delta\theta})_\theta = 0.5\frac{1}{\mathrm{r}\Delta\theta} N_L \rho\kappa F V_{\theta\max}^2 \qquad (11)$$

where $\Delta r, \Delta\theta$ are the dimensions of the computational cell. N_L is the number of tubes in cross flow in a given direction(r or θ), ρ is the density of the fluid, $V_{r\max}, V_{\theta\max}$ is the fluid velocity of the minimum area of cross section in the r direction and θ direction respectively. f is the friction factor, and x is a geometry factor dependent on the arrangement of tubes. Zukahauskas (1988) provided the charts for f and x. As for the friction along tube axis,, the pressure drop correlations of Rehme (1973) can be adopted:

$$R_Z = 0.5\frac{1}{\Delta Z} f \rho V_Z^2 \qquad (12)$$

where the friction factor is determined by

$$(\frac{8}{f})^{0.5} = A\left\{2.5\ln[\mathrm{Re}(\frac{f}{8})^{0.5}] + 5.5\right\} - G^* \qquad (13)$$

where A and G^* are geometry parameters given by Rehme(1973) which depend on the tube layout. Re is the Reynolds number based on the hydraulic diameter of the computational cell.

Tubes in the heat exchangers enhance the production and dissipation of turbulence kinetic energy. According to, Prithiviraj and Andrews(1998a,1998b) the turbulence generation due to the existence of tubes can be formulated as:

$$R_k = \int_V R\cdot\vec{V}dV = R_r|V_r| + R_\theta|V_\theta| + R_z|V_z| \qquad (14)$$

The resistance source of turbulence dissipation is deduced from a limiting case of a fully developed flow in a tube bundle as(Prithiviraj and Andrews, 1998a,1998b):

$$R_\varepsilon = 1.92\frac{\varepsilon}{k}R_k \qquad (15)$$

where R_r, R_θ and R_z are given by Equations (10),(11) and (12).

The Treatment of Tubes Bundles and Baffle in the Simulation of Temperature Field

In the simulation of shell-and-tube heat exchangers, the shell envelope can be considered as insulator. The energy conservation can be described that the heat lost by the shell-side fluid is gained by the tube-side fluid or, alternately, the heat lost by the tube-side fluid is gained by the shell-side fluid. In the distributed resistance approach, the shell-side fluid in a computational cell has an enthalpy H_s and the tube-side fluid has an enthalpy H_t. The heat source ϕ for a given computational cell is computed by integrating the heat source or sinks within the computational cell over the surface area of tubes *As*. The heat transfer can be given as:

$$\phi = \int_{As} k(\frac{H_t}{C_{P,t}} - \frac{H_s}{C_{P,s}})dA_s \qquad (16)$$

where k is the overall heat transfer coefficient, $C_{p,t}$、$C_{p,s}$are the shell-side and tube-side fluid specific capacity, respectively. The source term for the energy equation is obtained by integrating Equation (16):

$$S_T = kA_s(\frac{H_t}{C_{P,t}} - \frac{H_s}{C_{P,s}}) = kA_s(T_t - T_s) \qquad (17)$$

As for the tube-side, it is assumed that the tube-side flow in a shell-and-tube heat exchanger is fully developed. Since the flow within the tubes is in the axial direction and diffusion is negligible, the governing equation for tube-side flow is:

$$\phi = \rho W_t \frac{dH_t}{dz} = \rho C_{p,t} W_t \frac{dT_t}{dz} \qquad (18)$$

The overall heat transfer coefficient, k, can be obtained from shell-side heat transfer coefficient and the tube side coefficient which can be found from Zukauskas (1988) for bare tube banks and from Gnielinski (1977). Then for bare tube banks the overall heat transfer coefficient can be calculated by:

$$k = \frac{1}{(1/h_s) + (\frac{d_0}{d_0 - 2\delta_w})(1/h_t) + (\delta_w/\lambda_{th})} \qquad (19)$$

where the overall heat transfer coefficient is based on the outer surface area of the tube banks

NUMERICAL SIMULATION METHODS

The governing equations are discetized by the finite volume method. The convective term is discretized by the power-law scheme. The coupling between velocity and pressure is deal with by the SIMPLER algorithm based on a stagger grid, where scalar properties such as pressure and enthalpy are calculated at the center of computational cells, while cell faces are used for each of the velocity components. The resulting algebraic equations are solved by the alternative direction iteration method. The velocity fields are first solved and then is the temperature field.

Numerical simulations were conducted for following three heat exchangers:

(1) HEx with vertical baffles;
(2) HEx with helical baffles;
(3) HEx with finned tube banks.

In the following, the numerical results will be presented for the three heat exchangers in order, and comparisons with experimental data will be made whenever possible.

NUMERICAL RESULTS OF HEX WITH VERTICAL BAFFLES

Simulation Conditions and Definition of Shell-side Re

The simulation conditions are shown in Table 2.

Table 2 Simulation conditions for HEx with vertical baffles

No	Parameter	Description
1	Shell-side fluid	air
2	Tube-side fluid	water
3	Shell diameter	0.41m
4	Shell length	1.98m
5	Number of baffle	3,5,7,9
6	Baffle cut	25%
7	Tube diameter	0.015m
8	Number of tubes	325
9	Inlet/outlet diameter	0.148m
10	Tube side inlet temperature	353K
11	Shell-side inlet temperature	293K

A shell-side Reynolds number is defined as follows:

$$\mathrm{Re}_s = \frac{G_c \cdot d_t}{\eta} = \frac{\frac{1}{4}\pi D_{in}^2 \cdot \rho \cdot u_{in}}{[d_s - (\frac{d_s}{Pt})d_t] \cdot \frac{L}{N_{cross}}} \cdot \frac{d_t}{\eta} \qquad (16)$$

where G_C (kg/m^{2}s) is the mass velocity of the shell-side fluid in the minimum area of cross section along the centerline of the heat exchanger, P_t is the tube pitch and $N_{cross} = N + 1$.

Velocity, Temperature and Pressure Fields

Simulations were conducted for tube side Reynolds number of 2000 and shell side Reynolds number varying from 10000 to 100000. For Re_s=50000, the predicted velocity, pressure and temperature fields in the longitudinal cross section for the five baffles case are presented in Figs. 3 and 4, and the three fields in different axial cross sections are shown in Fig. 5, where z=0.22 m and 1.75 m are the cross sections of inlet and exit respectively. As seen in the figs., the fluid enters the heat exchanger at the inlet and sweeps back and forth across the tubes before it leaves out through the exit. The shell-side fluid velocities are high in the inlet and outlet regions because of the sudden expansion and contraction. For the case studied, no recirculation zones are formed near the baffles. For the case studied the pressure variation range is 150000Pa and the fluid temperature varies from 294K to 340K.

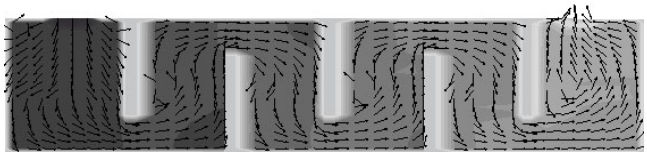

Fig. 3 Fluid velocity and pressure field

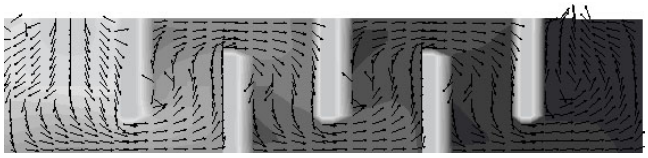

Fig. 4 Fluid velocity and temperature field

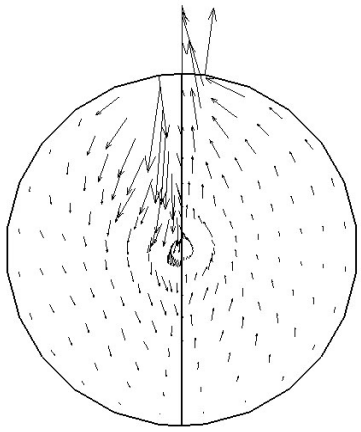

Z=0.22m Z=1.75m

(a) Flow fields

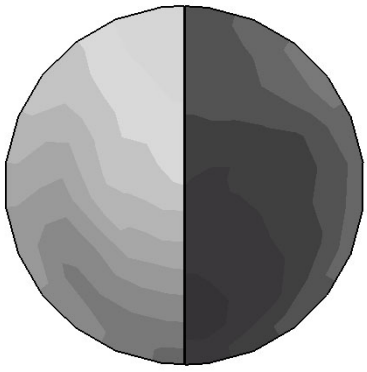

Z=0.22m Z=0.8m

(b) Temperature fields

Fig. 5 Cross-sectional velocity and temperature fields

In the two cross sections of z = 0.22 m and 0.8 m, the main flow goes from shell top to the bottom. Thus the shell side fluid temperature reaches its maximum at the bottom of the cross section as seen in Fig. 5(b).

The Effect of Re on Pressure Drop and Heat Transfer

For the case of five baffles, the variation of the shell side total pressure drop with Re_s is shown in Fig 6. The results can be well fitting by following equations;

$$\Delta p = 4.78\times10^{-4}\ \mathrm{Re}_s^{1.814} \quad (17)$$

This is in good agreement with fluid mechanics in that for the turbulent flow fluid pressure drop is proportional to the $u^{1.75}$ to $u^{2.0}$.

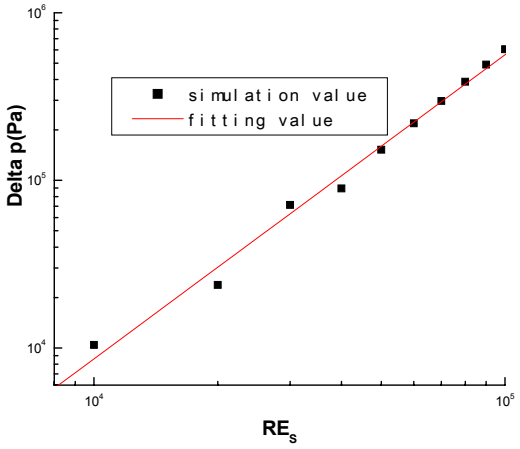

Fig. 6 Shell side pressure drop vs. Re_s

Pressure drop distributions in the above heat exchanger are presented in Figs. 7. The difference between point 1 and point 9 gives the overall pressure drop in the heat exchanger. As seen from the figure, there is a steady decrease in the pressure value as the fluid flows across the tubes in the heat exchanger, followed by a slight increase close to the outlet, the same phenomenon was found by Prithiviraj and Andrew(1998a,b). The pressure drop between inlet point 1 and point 2, outlet point 8 and point 9 is relatively large, because in the inlet and outlet part, flow area has a sudden expand and contract, resulting in relative large flow resistance.

Figure 7 shows the variation of shell side fluid mean temperature increase with the Reynolds number: ΔT_{shell} decreases gradually with the increase in Re_s. It can be observed from the figure that when the value of Re_s increases to 10 times the total heat transfer rate characterized by the production of $\Delta T_{shell}\times\mathrm{Re}_s$ increases to about 4 - 4.5 times. This implies that shell side thermal resistance is the dominated component.

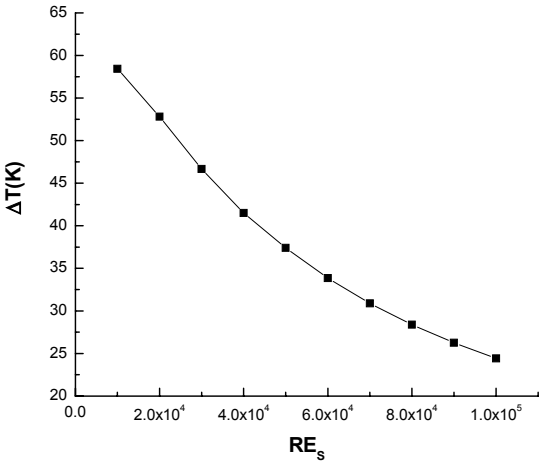

Fig. 7 Effect of Re_s on shell side temperature difference

Effect of Baffle Number on Δp_{shell} and ΔT_{shell}

Figure 8 shows that the effect of baffle number on pressure drop distribution in the heat exchanger under the same shell-side mass flow rate (U_{in} = 102.7m/s). As seen in the figure, under the same shell-side mass flow rate, with the increase in baffle number, the pressure drop between the inlet and outlet increases. However, in the regions of sudden expand and contract, the local resistance is the same for different baffle case because of the same mass flow rate and geometry structure. When the baffle number is small, the major pressure drop occurs in the inlet and outlet region.

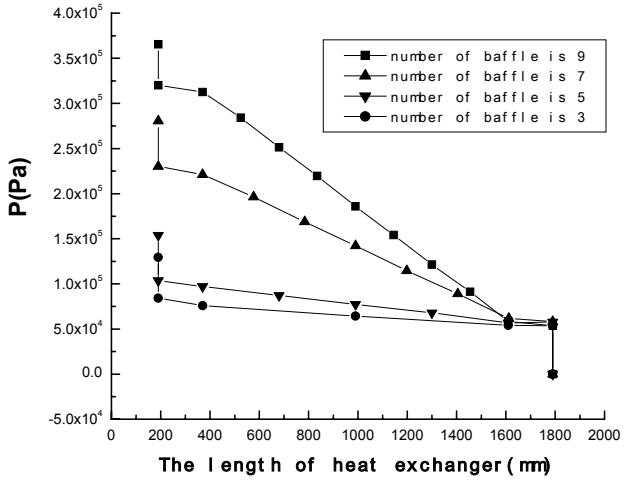

Fig. 8 Effect of baffle number on fluid pressure drop

Figure 9 shows the variation of shell side section average temperature difference between outlet and inlet with the baffle number. It can be seen that for a fixed shell side mass flow rate, the total temperature difference increases with the baffle number ,but the increase tendency gradually decreases. For the case studied, nine baffles are probably the maximum, beyond which increase in baffle

number will leads to the increase in pressure drop while no appreciable gain in heat transfer can be obtained.

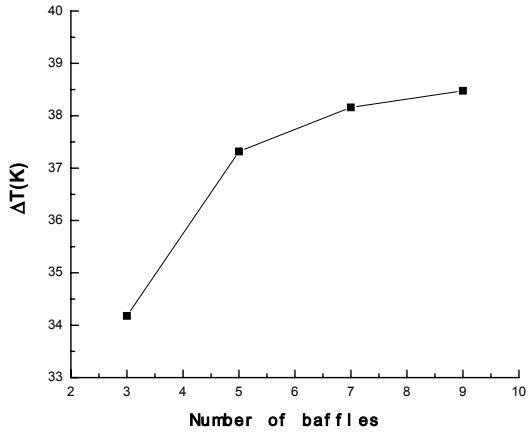

Fig. 9 Variation of shell side ΔT with baffle number

Experimental Validation of Pressure Drop Data

Three models of TEMA-E heat exchanger were made by plexiglass. The main characteristics of this heat exchanger is its simplicity: single shell and single tube side. The experimental apparatus is shown in Fig 10. In the heat exchanger model eleven pressure measuring taps were set up along the axial length, including the inlet and outlet sections. Air was used as the working fluid. The measured pressure drop variations along the axial length for six mass flow rate are presented in Fig. 11 for the case of 7 baffles. It can be seen that the agreement between predicted and measured pressure drop is quite satisfactory. The relative deviations are listed in Table 3. The maximum deviation occurs at the largest mass flow rate. It can be observed that the predicted pressure drops all larger than that of measured. This is

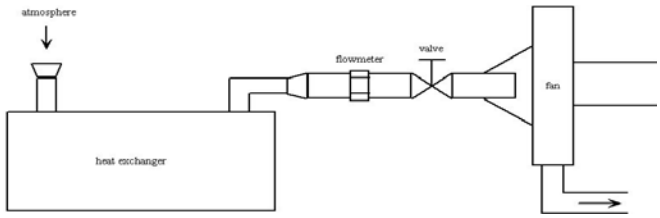

Fig. 10 Test apparatus for S-T HEx with vertical baffles

Table 3 Deviation of the predicted and test data for shell side total pressure drop

	$\Delta P / kPa$					
	1	2	3	4	5	6
Simulated	6.53	7.90	9.37	10.9	12.7	13.5
Test data	5.57	6.63	7.70	8.88	10.2	10.7
Deviation (%)	17.2	19.1	21.6	23.0	24.5	25.1

because in the practical model there are flow leaks through different paths, while in our numerical models these leaks are not taken into account.

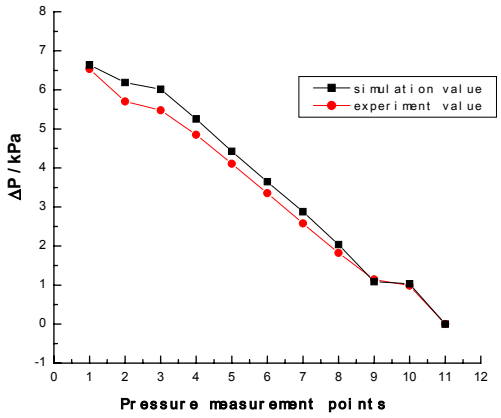

(a) Mass flow rate = 0.24 m^3/s

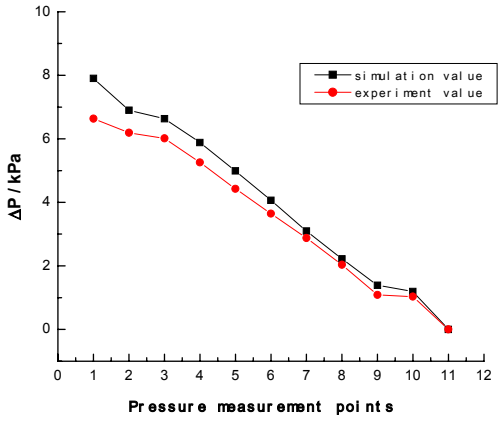

(b) Mass flow rate = 0.26 m^3/s

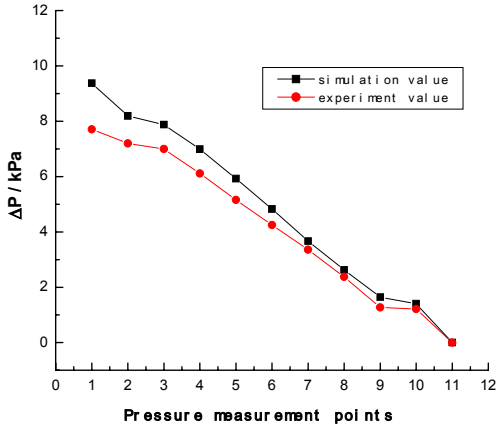

(c) Mass flow rate = 0.28 m^3/s

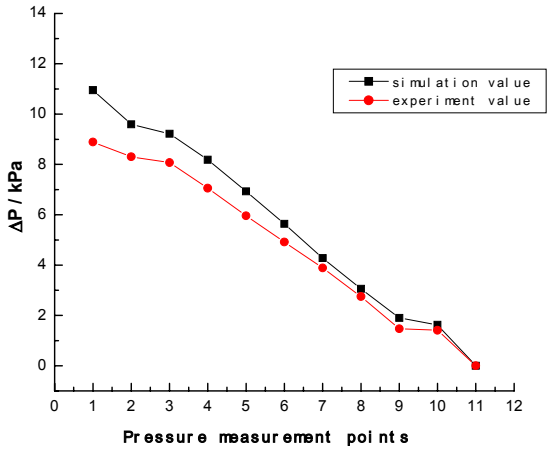

(d) Mass flow rate = 0.31 m^3/s

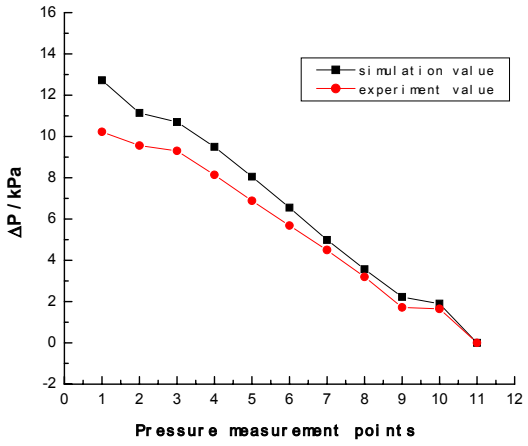

(e) Mass flow rate = 0.33 m^3/s

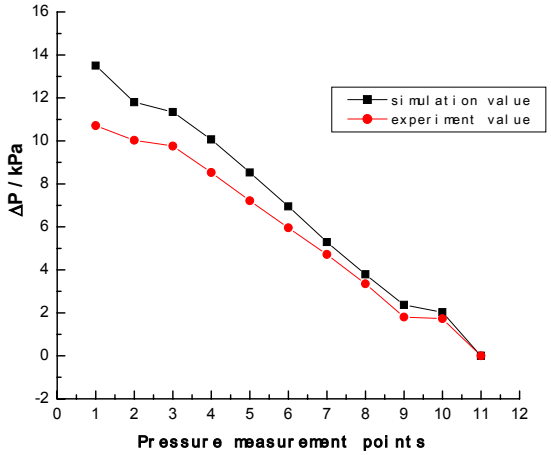

(f) Mass flow rate = 0.34 m^3/s

Fig. 10 Comparisons of predicted and measured pressure drops for heat exchanger with 7 baffles

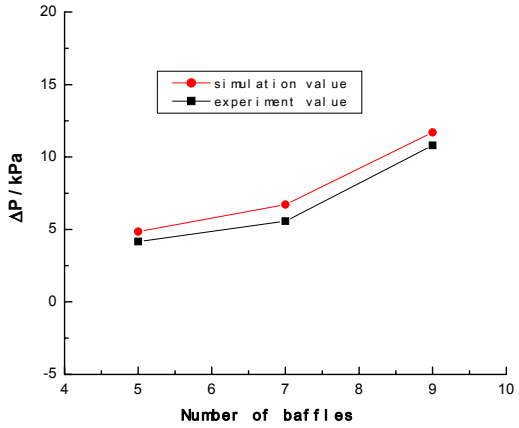

Fig.11 Effect of baffle number on the total pressured drop

The effect of baffle number on total pressure drop is shown in Fig. 11 for predicted and measured data at the mass flow rate of 0.24 m^3/s. The maximum deviation is 20.5%.

From above comparisons it can be concluded that the numerical methods and the code developed can predict flow characteristics with a reasonable good agreement.

In the following presentations, numerical results for shell and tube heat exchangers with helical baffles and finned tube banks will be presented. The major numerical methods and the same as that for the vertical baffles, hence will not be re-stated. Only those special numerical treatments for the individual case will be briefly mentioned.

NUMERICAL RESULTS OF HEX WITH HELICAL BAFFLES

Special Numerical Treatments

Because the helical configuration, the symmetry condition at the central longitudinal section can not be adopted anymore, rather, the whole region of the cylindrical space should be taken as the computational domain. In addition to meet the requirement for simulation of different baffle configurations, the most simple but useful method to deal with an irregular domain - stepwise approximation is adopted to simulate the baffle.

Reynolds Number Definition

In order to compare flow and heat transfer performance of heat exchanger with vertical and helical baffles, the shell-side Reynolds number is defined as follows:

$$\mathrm{Re} = \frac{u d_e}{\nu} \qquad (18)$$

where the characteristic dimension d_e takes the value of the tube diameter , u is the flow velocity in the minimum section, which is defined by Eq.(19):

$$u = \frac{q_{mo}}{\rho_o A_m} \tag{19}$$

In Eq.(19), A_m is the area of the minimum flow section, and q_{mo} is the shell side mass flow rate. The minimum flow area is determined by following equations for vertical baffles and helical baffles:

Vertical baffle: $A_{m,ver} = Bd_s(1-\frac{d_o}{p_t})$ (20a)

Helical baffle $A_{m,hel} = \frac{1}{2}Bd_s(1-\frac{d_o}{p_t})$ (20b)

where B is the distance between two adjacent baffles, d_s is the diameter of the shell, d_0 is the diameter of the heat transfer tube, and p_t is the tube spacing.

It is to be noted that the above definition of Re makes the numerical results comparable between those of vertical baffles and of helical baffles.

Helical Configurations Simulated

There are a lot of configurations of the helical baffle (B. Deng, 2003). The most fundamental configurations are presented in Figs. 12 and 13. For each figure the top picture is a pictorial view of the helical baffles and the bottom one is its simple presentation. In is study, the configurations shown by Fig. 12 and Fig.13(b) were simulated.

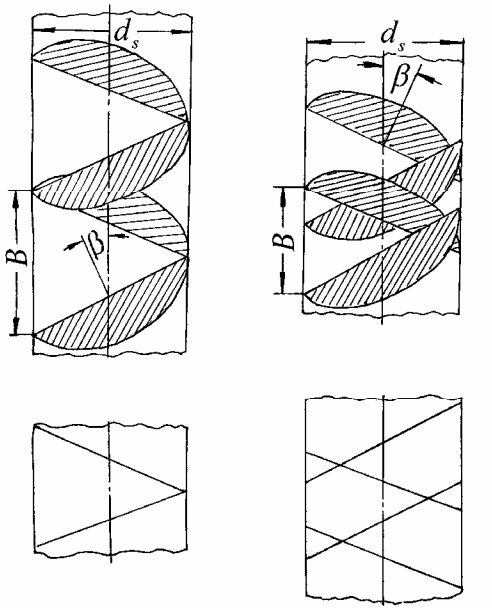

(a) Continuous half-ellipse baffle (b) Staggered half-ellipse baffle

Fig.12 Half-ellipse helical baffles

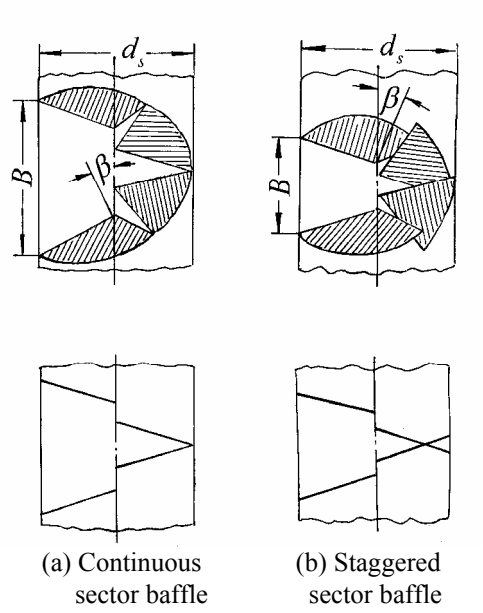

(a) Continuous sector baffle (b) Staggered sector baffle

Fig.13 Sector helical baffles

Numerical simulations were conducted for two combinations of working fluids: one is air (shell side)-water and the other is oil (shell side)-water. For the former kind the flow is usually in the turbulent regime and the modified $k-\varepsilon$ two-equation model was used, while for the later, shell side is usually in laminar flow and no turbulence model was incorporated.

Simulation Results of 1st Combination of Fluids

Simulation conditions are presented in Tables 4 and 5. For the simplicity of presentation, only the results of staggered half-ellipse baffle will be presented.

Table 4 Simulations conditions

Parameter	Description
Shell-side fluid	Air
Tube-side fluid	Water
Shell length	2.0 m
Shell diameter	0.6 m
Tube diameter	0.015 m
Tube pitch	0.020 m
Number of tubes	325
Diameter of inlet/outlet	0.20 m

Table 5 Baffle parameter

Baffle	Baffle pitch, B, m	Baffle number	Helical angle, degree
Helical „Fig. 12(a)	0.272	20	12,15,18
Helical „Fig. 12(b)	0.180	28	12,15,18
Vertical	0.140	9	0

The velocity distribution in a longitudinal cross section which transversely cuts the two half-ellipse baffles is presented in Fig. 14. As it can be seen in the figure, the fluid flow route is helical. The fluid flows through the empty space between the baffles, rushes to the shell wall of the heat exchangers, and part of it turns over to the other half of the heat exchangers then flows to the next circle..

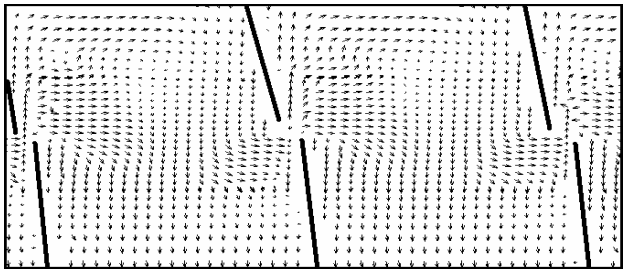

Fig. 14 Velocity distribution in a longitudinal cross section

In order to reveal the effect of helical angle on the total pressure drop, simulations were performed for three helical angles shown in Table 5, and the results are provided in Figs. 15, where the results for the vertical baffle are also presented for comparison. It can be clearly observed that compared with the shell-and-tube heat exchanger with vertical baffle the helical baffle can greatly reduce the pressure drop. And the larger the helical angle the smaller the pressure drop.

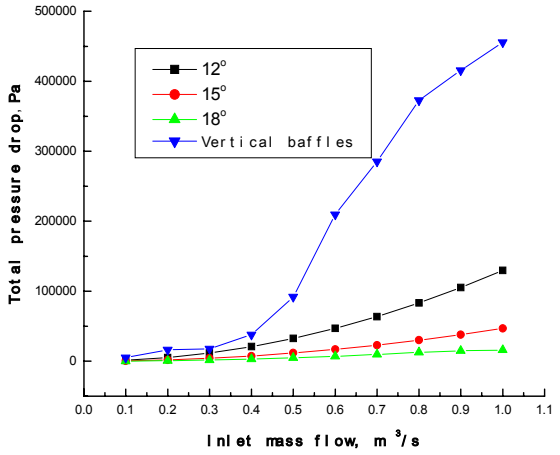

Fig. 15 Effect of helical angle on the pressure drop

Simulation and Test Results of 2nd Combination of Fluids

Two series of experimental measurements were conducted for the staggered sector helical baffle(Fig.13(b)), one for measurement of shell side pressure drop without heat transfer and the other for the measurement of heat transfer. The conditions of the two series of tests are summarized in Tables 6 and 7. The test system for heat transfer measurement is presented in Fig.16. For the measurement of pressure drop, only the oil loop was used. To take advantage of the test data, numerical simulations were performed accordingly.

Table 6 Test condition for pressure drop measurement

Parameter	Description
Length of heat exchangers	720mm
Diameter of shell	140mm
Diameter of tubes	10mm
Tube pitch	15mm
Number of tubes	69
Configuration of tube arrangement	square
Diameter of inlet tube	40mm
Diameter of outlet tube	40mm
Baffle pitch	68.4mm
Number of baffles	40

Table 7 Test conditions for heat transfer measurement

Parameter	Description
Shell diameter	182 mm
O/I tube diameter	10 / 7mm
Tube arrangement	Square
Tube thermal conductivity	36.7 W/m□K
Length of heat exchanger	1550 mm
Active length of tube	1139 mm
Tube number	72
Oil inlet tube ID	51 mm
Oil outlet tube ID	51 mm

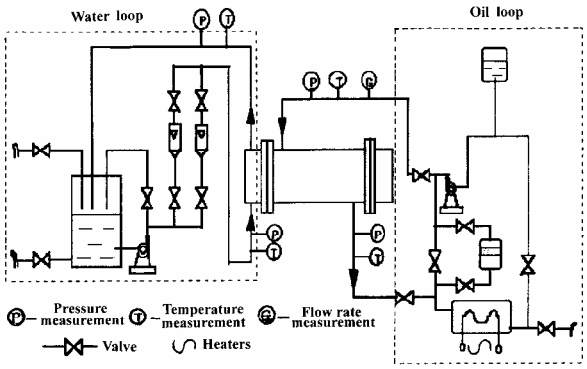

Fig. 16 Test system for heat transfer measurement

The comparison of pressure drops from measurement and simulation is shown in Fig. 17. It can be seen that within the mass flow rate of oil studied (2.0 m^3/h to 4.0 m^3/h) the agreement of the predicted and test data is quite good, with the maximum relative deviation of 18%.

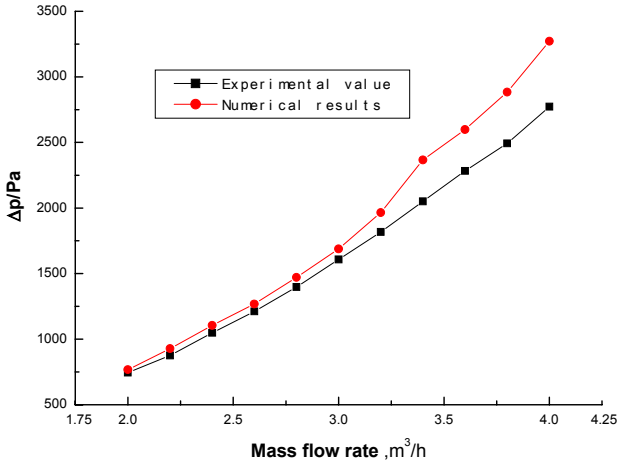

Fig. 17 Variation of pressure drop with mass flow rate

Table 7 Heat transfer results comparison

Point	1	2	3	4	5
Oil flow rate, kg/s	0.967	1.284	1.508	2.217	3.054
Water flow rate, l/s	4000	4000	4000	4000	4000
Oil inlet temp., ˚C	58.4	58.1	57.8	57.8	58.4
Oil outlet temp., ˚C	46.3	47.8	48.6	50.7	52.4
Water inlet temp., ˚C	14.6	15.0	15.8	17.9	18.2
Water outlet temp., ˚C	20.0	21.0	22.1	25.1	26.7
Simulated Oil outlet temp., ˚C	46.7 (3.3)	48.6 (7.8)	49.3 (9.9)	51.3 (8.5)	52.0 (-6.7)
Simulated water outlet temp., ˚C	19.4 (-11.1)	20.5 (-8.3)	21.7 (-6.3)	24.6 (-6.9)	27.1 (4.7)

The measured and predicted data for heat transfer are presented in Table 7, where for five data points, the predicted values of the outlet temperatures of the oil and water are listed. The number in the parentheses are the relative deviation based on temperature difference. It can be found that the agreement is quite good.

NUMERICAL RESULTS OF HEX WITH FINNED TUBE BANKS

Usually bare tubes are used in shell-and-tube heat exchangers. However, when the shell side fluid is air enhancement technique must be adopted to reduce the heat transfer surfaces. The most often adopted technique is to use finned tube bank, with an integrated fin sheet shared with a certain number of tubes. Such configuration is often used when the heat exchanger is used to cool air or gas with high pressure. Figure 18 presents such a heat exchanger which is widely used in Chinese factories as an air/gas intercooler. Numerical simulation was also performed with some special treatment of the shell side distributed resistance.

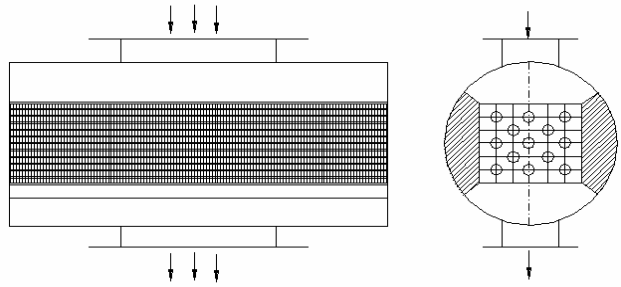

(a) Longitudinal cross section (b) Transverse section

Fig. 18 Shell-and-tube heat exchanger with finned tube bank

In Fig. 18(b) the shaded area is the blocked region so that the air steam go through the center part where finned tube banks are located. As far as the water side is concerned, two-pass arrangement was made in order to improve the local overall temperature difference distribution over the entire heat exchanger. This is shown in Fig. 19.

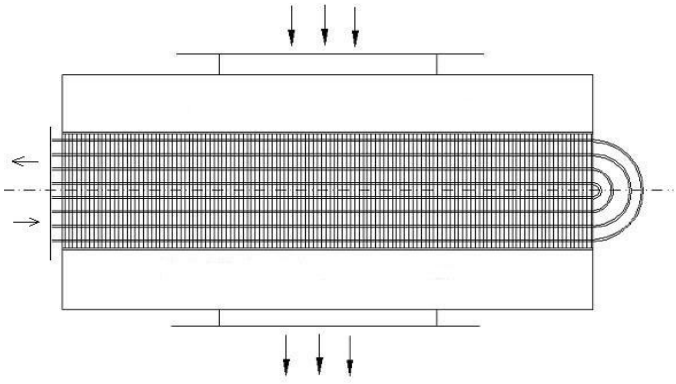

Fig. 19 Two-pass arrangement of water side

Obviously, in the finned tube bank region the axial gas flow can be totally neglected. This is numerically

implemented by setting $R_z = \infty$ (a very large number) in Eq.(12). In addition, no any baffles exist in the shell side. In the discretization of the computational domain, one has to be care of the axial control volume arrangement. Since the fin spacing is usually in the order of several millimeters, and the length of the heat exchanger is in meters, it is often impossible from computer memory consideration that each control volume only contains one piece of fin sheet. Often five to ten pieces of fin sheet should be included in one control volume in order to make the resulting algebraic equations manageable by a personal computer.

Determination of Distributed Resistances

From Eqs.(10), (11) it can be seen that in order to calculate the distributed resistances, R_r, R_θ the value of friction factor should be known. For the finned tube banks such as the one shown in Fig. 19, the general correlation resulted from bare tube banks can not be used. To this end, special test was arranged to obtain the friction factor correlation. Following result was obtained:

$$\lg f = 7.3389 - 3.6004 \lg(\mathrm{Re}_{\max}) + 0.42125(\lg \mathrm{Re}_{\max})^2 \quad (21)$$

where $\mathrm{Re}_{\max}$ is defined as follows:

$$\mathrm{Re}_{\max} = \frac{u_{\max} d_o}{\nu} \quad (22)$$

In Eq.(22) $u_{\max}$ is the maximum average gas velocity occurring at the minimum flow area.

Simulation Conditions

Simulation conditions were copied from a practical air intercooler which are listed in Table 8. As indicated in the table there are 870 pieces of fin sheet. *7 control volumes were used in the finned tube region such that each control volume includes 10 pieces of fin sheets.

Table 8 Simulation conditions for finned tube HEx

Parameter	Description
Shell-side fluid	air
Tube-side fluid	water
Shell diameter	0.734 m
Shell length	1.74 m
Fin thickness	0.00015 m
Fin spacing	0.00185 m
Fin Number	870
Tube diameter	0.0125 m
Tube spacing	0.032 m
Tube number	132

Velocity, Pressure and Temperature Distributions

For $\mathrm{Re}_{\max}$ = 20000 and tube side Re = 10000, the predicted velocity, pressure and temperature distributions in the longitudinal symmetric section are shown in Figs. 20 and 21. In the figures, the relative variation range of pressure is 0-80000Pa, and the variation range of air temperature is 347K ~ 353K. It can be observed following features. (1) In the middle cross section the air pressure drop is the largest because the highest downward air velocity in this region. (2) The cooling effect of the middle part of the finned tube

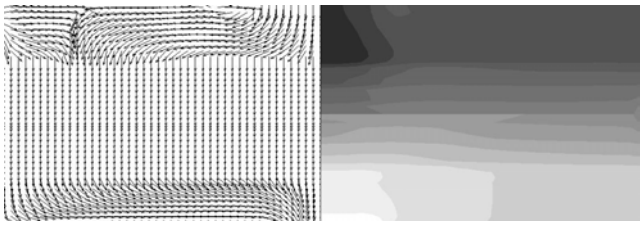

Fig. 20 Velocity and pressure distributions

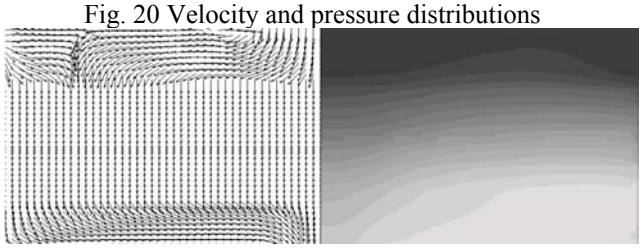

Fig. 21 Velocity and temperature distributions

is the worst. Although in the middle part the air side heat transfer coefficient is the largest compared with other part of the heat exchanger, the enhancement extent of heat transfer can not compensate the largest local flow rate of the air. Thus even though the local heat transfer rate is larger than anywhere else in the heat exchanger, the local exit temperature of the air is the largest. This result and that mentioned above for pressure drop may be an indication that the air distribution in the inlet region of the heat exchanger needs to be improved such that in the exit region the uniformity of air temperature and pressure can be better.

The effect of shell side Reynolds number on the total pressure drop is presented in Fig. 22 for the case of tube side Reynolds number =10000. By carefully inspecting the figure, it can be found that the increase of pressure drop with the increase in shell side Re is very significant, much faster than of the flow in ducts and across tube banks. As indicated in the figure the increase in flow rate from Re=10000 to Re=20000 leads to an increase in pressure drop from around 17000 Pa to 80000 Pa. Estimated by these two data, the exponent in the Reynolds number is about 3.5 to 3.6, instead of 1.75 to 2.0(see Eq.(17)). This may be accounted by the fact that the existence of the fin sheet greatly increases the frictional resistance to the flow across the finned tube bank.

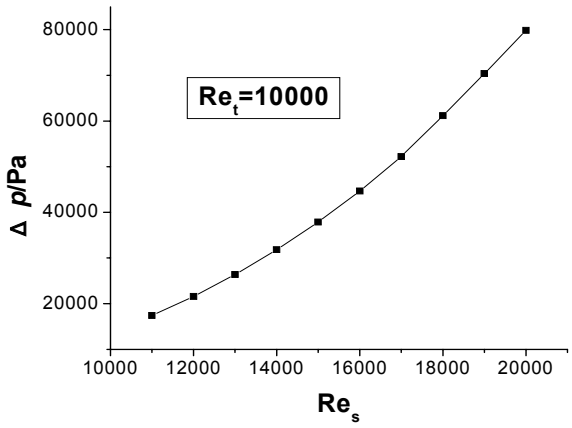

Fig. 22 Variation of pressure drop with Re

The effect of shell side Reynolds number on the heat transfer rate is shown in Fig. 23. It can be seen that the heat transfer rate increases with Re almost linearly, implying that even for the finned tube banks the airside thermal resistance is still a dominated component in the total thermal resistance compared with the water side resistance component.

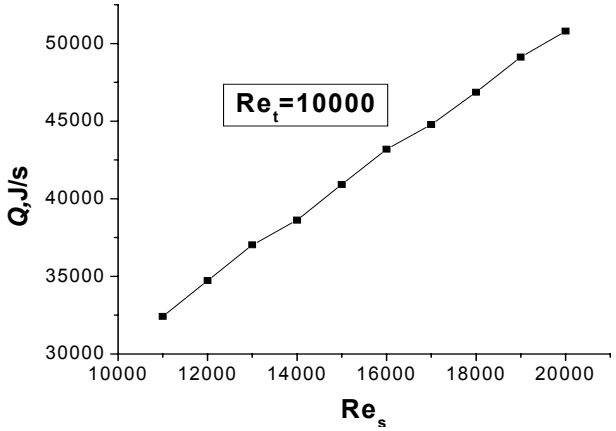

Fig. 23 Variation of heat transfer rate with shell side Re

CONCLUSIONS

In this keynote lecture for numerically predict heat transfer and flow characteristics of shell side fluid in shell-and-tube heat exchangers, a modified porous medium model in conjunction with distributed resistance and two-equation $k-\varepsilon$ closure was presented in detail. The model and developed codes were used to simulate three kinds of shell-and-tube heat exchangers (vertical baffles, helical baffles and finned tube banks), and comparisons were made between the predicted results and test data specially obtained in the authors group to verify the model. Generally speaking reasonably good agreements were received. Although such model requires that the friction factor correlation is known for the shell side fluid, it can still provide useful information for the shell side fluid flow and heat transfer and is a useful tool in the design of heat exchangers.

Further research needs to be performed includes the accumulation of more reliable friction factor correlations. In the numerical algorithm aspect, development of a new computational system which possesses a much faster convergence rate with enough numerical accuracy and stability is highly required.

ACKNOWLEDGMENTS

The work reported here was supported by following foundations: National Natural Foundation of China (No. 50476046, 50425620, 50236010); A Foundation for the Author of National Excellent Doctorial Dissertation of P R China; and RFDP20030698015.

REFERENCES

Bell K J. Final report of the cooperative research program on shell-and-tube heat exchangers. Bulletin No. 5. University of delaware engineering experimental station, Newark, Delaware, 1963

Butterworth D. A model for heat transfer during three-dimensional flow in tube bundles. Paper HX-6, 6th Int. Heat Transfer Conf. , Aug. 1978, Toronto

Deng B. Experimental and numerical study of flow and heat transfer in the shell side of heat exchangers. Ph D. Thesis. Xi'an Jiaotong University, Xi'an, China, 2003

Halle H, Cheoweth J M, Wambsganss M W. Shell side water flow pressure drop distribution measurements in an industrial-sized test heat exchanger. In: A reappraisal of shell side tube flow in heat exchangers, 22nd Heat Transfer Conference and Exhibition, Niagara Falls, ASME, HTD. 1984, 39: 37~48

Palen J W, Taborek J. Solution of shell side flow pressure drop and heat transfer by stream analysis method. Chem. Eng. Prog. Symp. Ser., 1969, 65(93): 53~63

Patankar S V. Numerical prediction of shell side flow and heat transfer in heat exchangers. In: A reappraisal of shell side tube flow in heat exchangers, 22nd Heat Transfer Conference and Exhibition, Niagara Falls, ASME, HTD 1984, 39: 1~9

Patankar S.V., Spalding D.B. A calculation procedure for transient and steady state behavior of shell-and-tube heat exchanger. In: Afgan N.F., Schlunder E.U., eds. Heat exchanger: design and theory source book, McGraw-Hill, New York, 1974

Pletcher L S, Andrews M J. Technical/market assessment of heat exchanger technology for users of natural gas. GRI Report GRI-94/0248. 1994

Prithiviraj M, Andrews M J. Three dimensional numerical simulation of shell-and-tube heat exchangers. Part I: Foundation and Fluid Mechanics. Numerical Heat Transfer, 1998a, 33A: 799~816

Prithiviraj M, Andrews M J. Three dimensional numerical simulation of shell-and-tube heat exchangers.

Part II: Heat Transfer. Numerical Heat Transfer, 1998b, 33A: 817~828

Rehme K. Simple Method of prediction factors of turbulent flow in noncircular channels. Int. J. Heat Mass Transfer, 1973, 16: 933~950

Sha W T, Yang C I, Kao T T, et al. Multi-dimensional numerical modeling of heat exchangers. ASME J. Heat Transfer, 1982, 104: 417~425

Sha W T. Numerical modeling of heat exchangers. In: Cheremisinoff N P, ed. Handbook of Heat and Mass Transfer, Gulf Publishing, 1985, 1

Tao W.Q. Numerical heat transfer. 2nd edition. Xi'an Jiaotong University Press, Xi'an, 2001

Tinker T. Shell-side characteristics of shell-and-tube heat exchangers: A simplified rating system for commercial heat exchangers. Trans. ASME, 1958, 36~52

Zukauskas A. Convective heat transfer in heat exchangers. Science Press, Moscow,1982